X-622-69-313
PREPRINT

THE ACCURACY OF THE HIGH RESOLUTION INFRARED RADIOMETER ON NIMBUS II

E. J. WILLIAMSON

AUGUST 1969

GODDARD SPACE FLIGHT CENTER
GREENBELT, MARYLAND

X-622-69-313
PREPRINT

THE ACCURACY OF THE HIGH RESOLUTION INFRARED RADIOMETER ON NIMBUS II

E. J. Williamson

August 1969

GODDARD SPACE FLIGHT CENTER
Greenbelt, Maryland

CONTENTS

THE ACCURACY OF THE HIGH RESOLUTION INFRARED RADIOMETER ON NIMBUS II

by
E. J. Williamson*
Goddard Space Flight Center

INTRODUCTION

Following the launch of Nimbus II on May 15, 1966, the High Resolution Infrared Radiometer (HRIR) provided measurements of surface and cloud-top temperatures for a total of 2455 orbits until November 15, 1966 when the tape recorder on the satellite failed and prevented further use of the instrument (Reference 1). The data gathered during this period have provided meteorologists and geophysicists with much valuable information and have made possible the nighttime mapping of clouds. It is in connection with the mapping procedure that this study of HRIR noise has been carried out.

DESCRIPTION OF THE INSTRUMENT

The HRIR is a scanning radiometer with an instantaneous field of view of 0.5 degree. It operates in the 3.8-micron atmospheric window region of the spectrum. The scanning mechanism consists of a mirror mounted at 45 degrees to an axis of rotation along the spacecraft velocity vector. The scan rate of 44.7 rpm is chosen to obtain contiguous scanning along the subsatellite track. One complete rotation of the scan mirror takes 1.342 seconds during which time it views, in turn, earth, space, and the radiometer housing which comprises an internal calibration target. The video signal from the instrument has an information bandwidth of 280 Hz and is recorded in analog form on a tape recorder within the satellite.

The procedure for reducing the data has been described in detail elsewhere (Reference 2). Video signals stored within the satellite are transmitted on command and recorded in analog form on the ground. The analog tape is digitized subsequently at a rate corresponding to 1000 samples per second of original recording time, producing 1342 samples for each scan. This raw digital tape forms the input to the HRIR calibration program that extracts the earth portion of the scan, converts radiance values to equivalent black-body temperatures, and inserts orbital and attitude

*On leave from the University of Oxford, England, as a National Academy of Sciences–National Research Council Postdoctoral Resident Research Associate.

information. The end result is the Nimbus Meteorological Radiation tape (NMRT) for the HRIR. The data are made available to the user in this form.

THE GRID-PRINT MAP

Perhaps the main use of HRIR data has been the production of grid-print maps for the study of cloud and surface features. The grid-print map is produced by the computer from the relevant NMRTs and consists of equivalent black-body temperatures printed on a half-inch mesh in the form of a polar or Mercator projection. Scales of 1:2,000,000 and 1:10,000,000 are in common use for the synoptic study of cloud systems and sea surface temperature (References 3 and 4). In these cases, the mesh size is such that each temperature value is generally an average of 10 or more HRIR data points. The effect of instrumental noise is thus considerably reduced and, in general, can be neglected.

Recent applications have demanded more detailed maps, and scales of 1:1,000,000 and 1:500,000 have been produced. The effect of noise in the data cannot now be ignored since little averaging takes place, and, in the limiting case, a point on the grid-print map is a single HRIR data point. It is therefore important to examine quantitatively the magnitude of the noise present within the raw data and its variation with target temperature.

SOURCES OF NOISE IN THE HRIR

It has been known for some time that the HRIR video signal contains both periodic and random noise components. The former consists mainly of a 200-Hz waveform caused by pickup from the spacecraft clock. It can be removed largely by numerical filtering, and a subroutine devised by McMillin (Reference 5) forms part of the standard mapping program. On the other hand, random fluctuations can be reduced by smoothing—but, of course, at the expense of spatial resolution.

No indication of the instrumental noise level is provided on the NMRT, nor can its value be deduced from NMRT data since it is not possible to separate, with confidence, those fluctuations caused by radiative changes from those caused by noise. Therefore, it has been necessary to analyze raw digital records.

Figure 1 shows an analog trace of one complete scan of the radiometer. Time and rotation angles are measured from the beginning of the first synchronizing pulse. It can be seen that the noise level present during the space portion of the scan is considerably larger than that which exists when the instrument is viewing the housing. These portions of the scan correspond to constant radiance levels and therefore can be assumed to indicate true instrumental noise. The difference in noise level is caused by the nonlinear characteristic of the amplifier within the instrument which is used to compensate for the nonlinear dependence of radiance on temperature at 3.8 microns. It takes the form of a transition from a linear characteristic to an almost logarithmic one for signal levels corresponding to target temperatures above approximately 240°K.

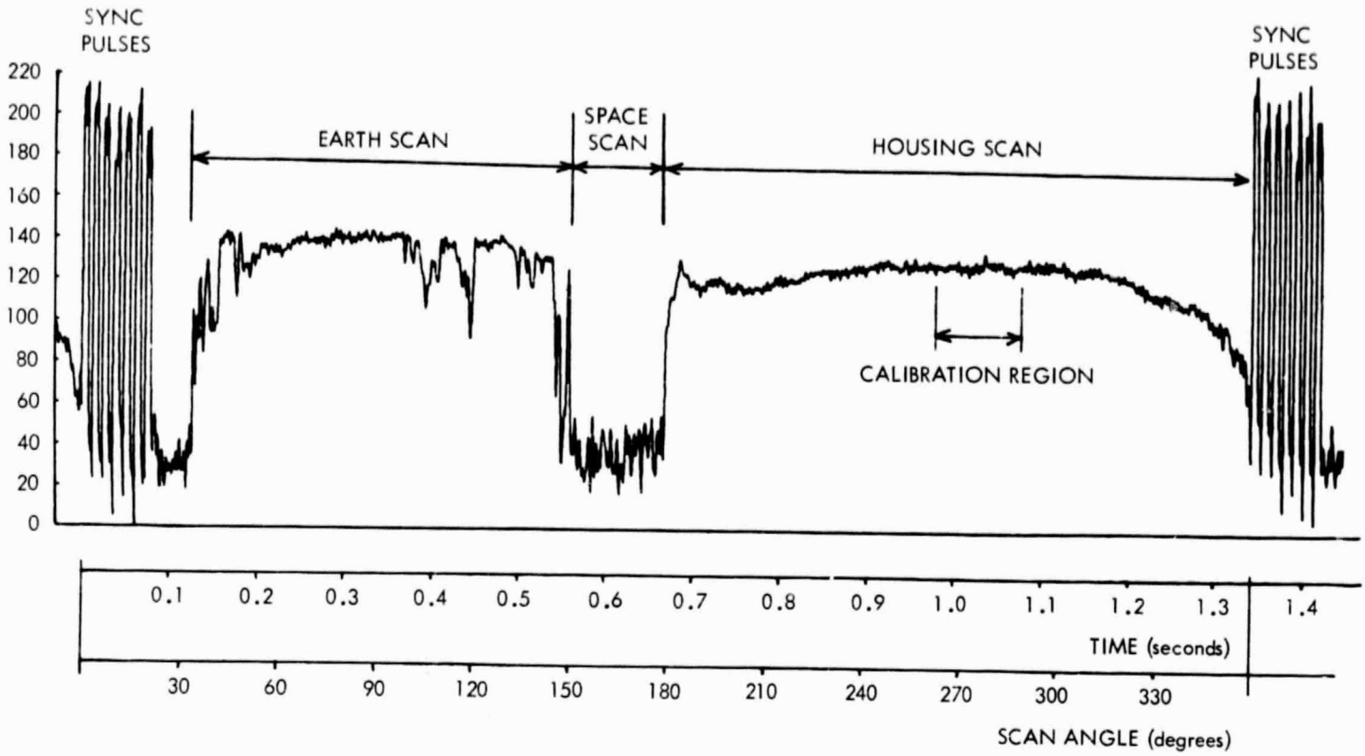

Figure 1—One complete scan of Nimbus II HRIR data from orbit 327 at time 19H 46M 9S UT plotted directly from the raw digital data.

CALCULATION OF NEΔT

The Noise Equivalent Temperature Difference (NEΔT) for a radiometric measurement is defined as that change in target temperature that would produce a change in measured response equal to the rms noise at the output of the instrument.

The measured response D (digital counts) is related to the target temperature T by

$$D = N(T)\,\omega A \tau R\, G(T)\, k + Z ,$$

where

$N(T)$ is the Planck radiance for spectral region concerned,

ω is the instantaneous solid angle of view,

A is the effective area of the entrance aperture,

τ is the net transmission of the optical system,

R is the detector responsivity,

$G(T)$ is the normalized amplifier nonlinear gain factor,

k is a factor containing constant-gain components and the conversion to digital response,

Z is the zero level offset.

The foregoing expression implies a continuous dependence of D on T although, of course, D is quantized in the digitization process. Quantization errors are discussed later.

If we express radiance in units of digital response N_D as measured through the system with a gain factor G = 1, we may write

$$D = G(T)\, N_D(T) + Z .$$

The measured noise can be regarded as a combination of two components,

1. That introduced before the nonlinear amplifier, the size of which will depend on the magnitude of the signal, and
2. That introduced at the output, which will be constant. We will call these two components γ_1 and γ_2 respectively, the units in each case being rms digital response as measured at the output.

A change in D caused by a change in N_D is given by

$$\Delta D = \left(\frac{\partial D}{\partial T}\Big/\frac{\partial N_D}{\partial T}\right)\Delta N_D$$

$$= \left(G(T) + N_D \frac{\partial G}{\partial T}\Big/\frac{\partial N_D}{\partial T}\right)\Delta N_D .$$

The expression in parentheses represents the effective gain of the system to noise as a function of target temperature. We will denote this by G_N. Since $\partial G/\partial T$ is negative or zero, then, in general, the signal-to-noise ratio is larger at the output than at the input—although signal-to-noise ratio is not a meaningful concept when dealing with a nonlinear system.

We can now equate ΔN_D with γ_1 and write an expression for the total noise ΔD_T at the output. Assuming that the contributions are uncorrelated, we have

$$\Delta D_T^2 = \gamma_2^2 + \Delta D^2$$

$$= \gamma_2^2 + G_N^2 \gamma_1^2 ;$$

G_N can be deduced as follows. Figure 2 shows the calibration curve for the Nimbus II HRIR operating with a detector temperature of -66.7°C. It is one of a set of curves for different detector temperatures used by the computer program that generates the NMRT. Measurements of detector operating temperature made throughout the lifetime of the epxeriment showed a variation of only 1 or 2 degrees from -66°C. It can be seen that the output approaches a constant offset value at low temperatures as the radiance tends toward zero. Figure 3 shows the same curve plotted on a

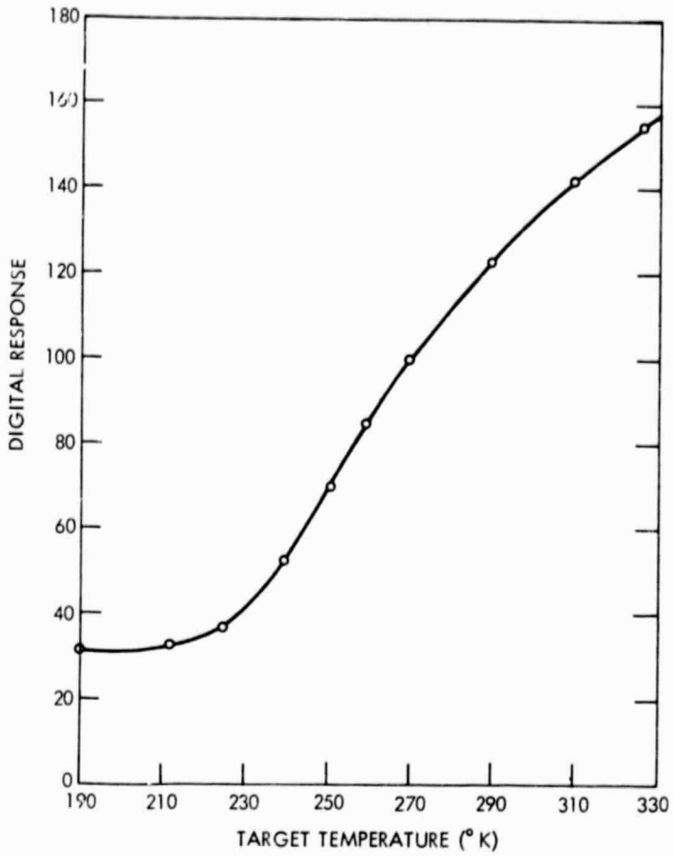

Figure 2—Nimbus II HRIR calibration curve for -66.7°C detector as used in current data analysis program.

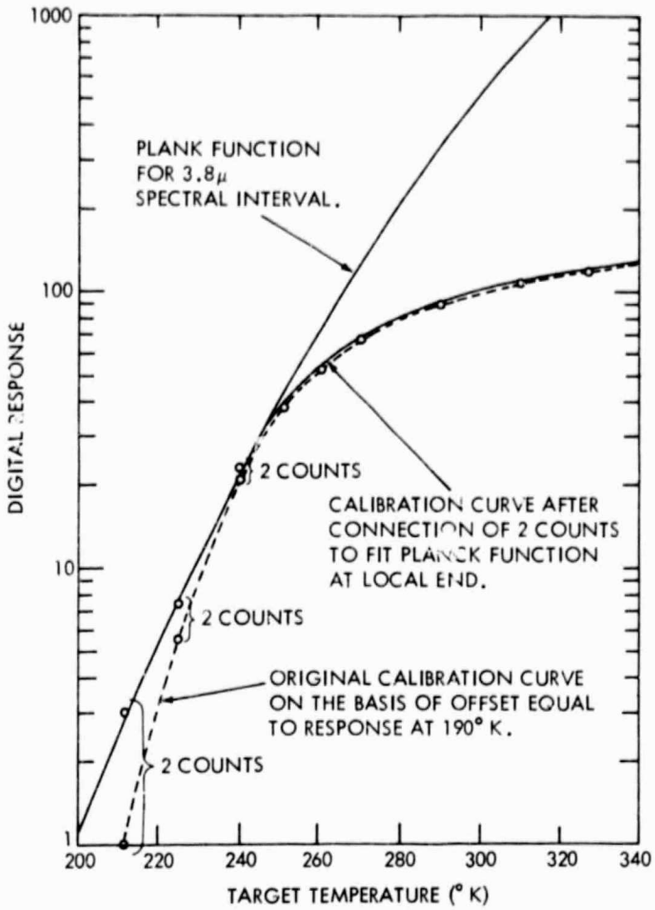

Figure 3—Nimbus II HRIR calibration curve for -66.7°C detector plotted on logarithmic scale with region below 240°K made to conform to shape of Planck function.

logarithmic scale with the offset removed. Since we know that the amplifier approaches a linear response for target temperatures below 240°K, the curve in this region must follow the shape of the temperature-dependence of the Planck function, integrated over the spectral passband of the instrument. The exact offset value has been chosen to obtain this fit. The Planck temperature function, also plotted in Figure 3, shows what the instrument's response would be if the amplifier gain were maintained at a constant value. The ratio of the two curves gives the relative signal gain G, and the ratio of their gradients gives the effective noise gain G_N as a function of target temperature. These are shown in Figure 4.

Measurements on space and housing portions of 10 scans taken throughout the operating lifetime of the experiment are shown in Table 1. The average noise level on the housing scan is 1.88 rms digital counts and on the space scan, 9.16 counts. The lower noise level at housing temperature is caused by the gain reduction at this signal level. These two results enable us to determine the values of γ_1 and γ_2.

We have, for the housing level, at temperature T_H = 294°K, and with $G_N(294) = 0.06$

$$\gamma_1^2 G_N(T_H)^2 + \gamma_2^2 = 1.88^2 ,$$

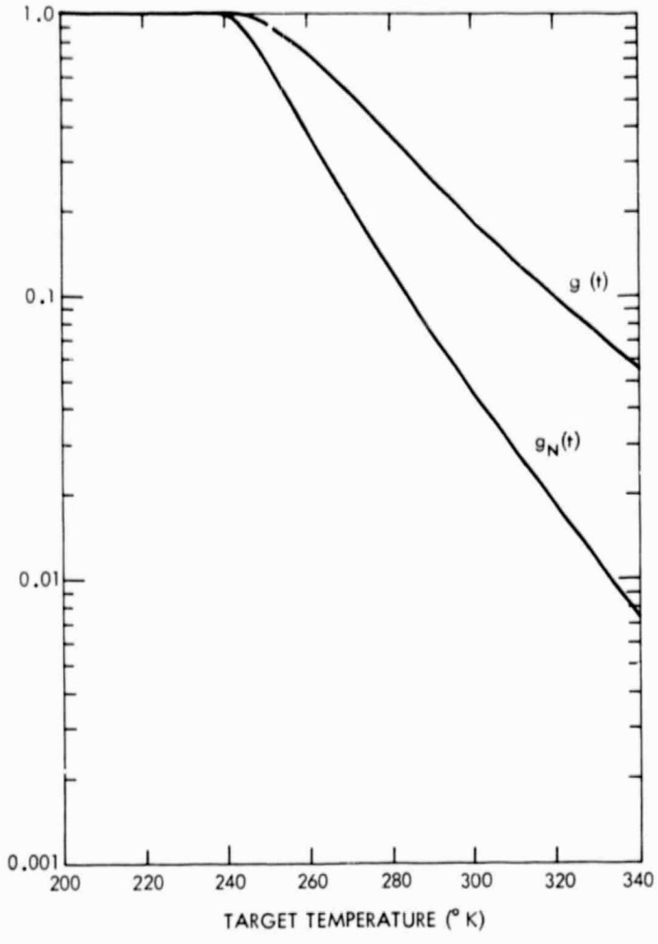

Figure 4—The functions G(T) and $G_N(T)$ deduced from calibration curve.

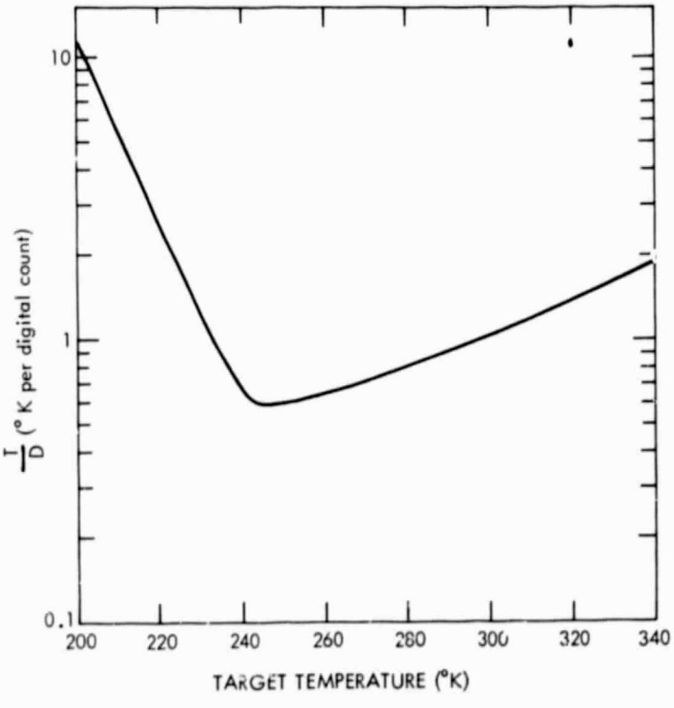

Figure 5—The function $\partial T/\partial D$ computed from the gradient of the calibration curve.

Table 1

HRIR Noise Measurements

Housing Scans					
Orbit number	Time (sec)	Raw data		Filtered data	
		Mean level	Standard deviation	Mean level	Standard deviation
191	54453	127.6	1.59	127.8	1.29
191	54455	127.8	1.75	127.7	1.29
327	71167	128.0	1.41	128.0	0.98
563	49788	122.8	2.07	122.7	1.63
563	49790	122.8	2.36	122.7	1.47
563	49791	123.2	2.29	123.2	1.76
1253	38158	119.7	1.66	119.7	0.95
1917	21835	116.6	2.07	116.6	2.07
2157	04326	123.4	1.85	123.4	1.18
2157	04327	122.5	1.77	122.7	1.24
Averages		123.4	1.88	123.4	1.35
Space Scans					
Orbit number	Time (sec)	Raw data		Filtered data	
		Mean level	Standard deviation	Mean level	Standard deviation
191	54452	31.2	8.74	31.2	6.42
191	54456	30.6	8.65	30.5	6.89
563	49788	32.3	8.48	32.3	6.88
563	49789	32.1	8.67	32.0	5.97
563	49791	29.4	9.55	29.3	7.41
1253	38159	30.5	9.74	30.6	7.61
1917	21658	34.9	9.14	34.8	6.87
1917	21801	27.0	10.49	27.0	7.34
2157	04327	41.5	8.04	41.7	5.90
2157	04327	38.4	10.17	38.4	8.49
Averages		32.8	9.16	32.8	6.98

and for the space level, since the effective gain is unity,

$$\gamma_1^2 + \gamma_2^2 = 9.16^2 .$$

Simultaneous solution yields $\gamma_1 = 8.98$ and $\gamma_2 = 1.80$ rms digital counts.

We are now in a position to calculate NEΔT as a function of target temperature. It is given by

$$NE\Delta T = \frac{\partial T}{\partial D} \Delta D_T$$

$$= \frac{\partial T}{\partial D} \sqrt{\gamma_1^2 G_N^2 (T) + \gamma_2^2} \quad ;$$

$\partial T/\partial D$ is the inverse gradient of the digital calibration curve and is plotted in Figure 5. It expresses the temperature change corresponding to one digital count as a function of target temperature. The NEΔT is plotted in Figure 6.

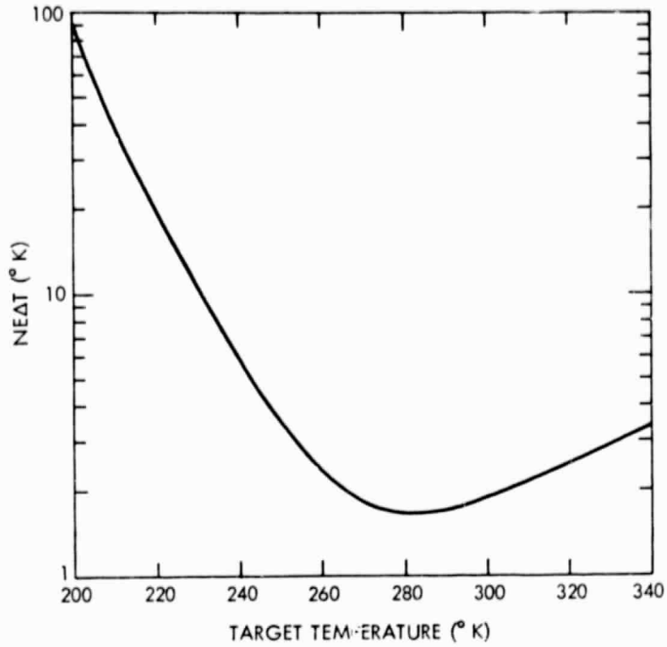

Figure 6—Noise equivalent temperature difference (NEΔT) for Nimbus II HRIR as a function of target temperature.

QUANTIZATION ERRORS

The minimum noise level at the output will be equal to γ_2 or 1.8 rms digital counts. At high temperatures, quantization error will represent a significant fraction of the uncertainty in a single data point, being in the region of 1°C at 300°K (see Figure 5). However, the random noise level is sufficiently high that this error can be reduced by averaging, provided that the digitization levels are sufficiently accurate to carry the extra information.

NUMERICAL FILTERING

The effect of the 200-Hz component in the noise level of the housing and space portions of the scan has been investigated, using McMillin's filter (Reference 5). The results are shown in Table 1. It can be seen that the filter reduces the overall noise level in each case by about 25 percent. Values of NEΔT for filtered data will be reduced by the same amount. McMillin's filter operates on temperatures from the NMRT, whereas a more realistic procedure would be to operate directly on the raw digital data. A Fourier technique recently developed by Forman* would provide a versatile means of performing such an operation on future data.

*Forman, M. L., Goddard Space Flight Center, Private communication, 1968.

TEMPERATURE-AVERAGING

So far we have considered only errors associated with instrumental noise. There are, however, two other sources of error that may be introduced during data reduction. Both are systematic and arise from the averaging of temperatures rather than radiance.

Nonlinear Averaging

The temperature T_i indicated by a single HRIR measurement D_i will be

$$T_i = E(D_i) ,$$

where the function E represents the calibration curve (see Figure 2) relating temperature to digital response with D_i regarded as the independent variable. We now express D_i in terms of the deviation ΔD_i from the mean digital level $\langle D \rangle$ and expand the function in the form of a Taylor series, neglecting terms beyond the third.

$$T_i = E(\langle D \rangle) + \frac{\partial}{\partial D} E(\langle D \rangle) \Delta D_i + \frac{\partial^2 E}{\partial D^2} (\langle D \rangle) \frac{\Delta D_i^2}{2} + \cdots .$$

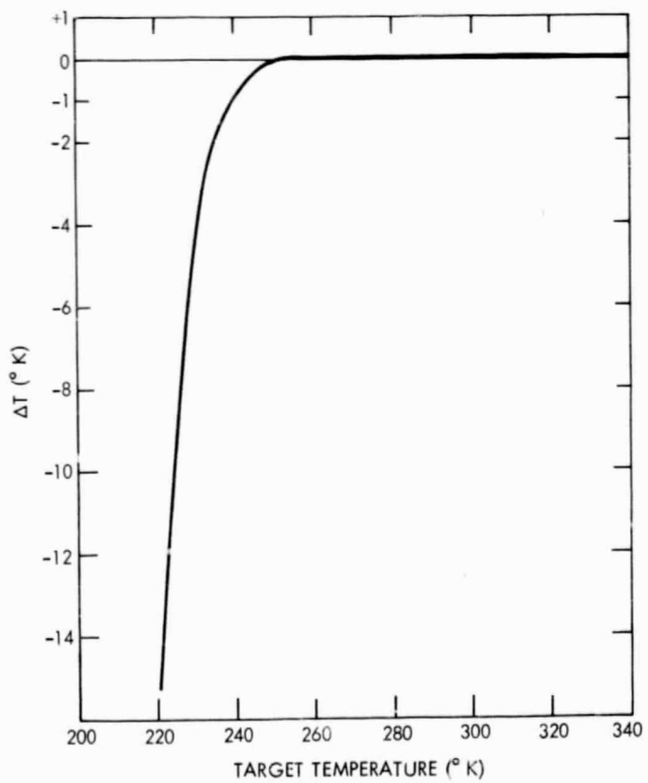

Figure 7—Systematic temperature error caused by nonlinear averaging.

Taking the average over N measurements gives

$$\langle \tau \rangle - E(\langle D \rangle) = 0 + \frac{1}{2} \frac{\partial^2 E}{\partial D^2} (\langle D \rangle) \frac{1}{N} \sum_{i=1}^{N} \Delta D_i^2 .$$

This equation expresses the difference between the mean of the indicated temperature values and the temperature corresponding to the mean digital value, in terms of the digital noise level and the second derivative of the calibration curve. The error is thus largest at low temperatures where the curvature is greatest. The function $\partial^2 E/\partial D^2$ can be expressed as $\partial/\partial T \; (\partial T/\partial D) \; \partial T/\partial D$ and obtained from Figure 5. The result is shown in Figure 7. Near 250°K, the error is positive and less than 0.1°K. At 240°K, the measured mean temperature is lower than the true temperature by about 0.7°, and the error increases rapidly at lower temperatures.

The Cutoff Level

A second and more serious error arises from the practice of employing a cutoff temperature as a consequence of the inflight calibration. The zero radiance level is measured by averaging the space portion of all scans throughout an orbit. This level may differ from the 190°K value on the calibration curve (which essentially corresponds to zero radiance) because of a shift in the offset value. In this case, a cutoff is defined by the space level and temperatures corresponding to measured values below that level are set at 190°. The cutoff level may be as high as 230°K.

Because the noise level at low temperatures is in the region of 9 counts rms, then, unless the target temperature is above approximately 240°, some noise peaks will result in digital values corresponding to temperatures below the cutoff. At low temperatures, this is especially important because a significant fraction of the data may be affected.

The data available to the user are thus biased at low temperatures. The 190° values contain no quantitative information except to indicate that a measurement has fallen below the cutoff level. In one of its versions, the mapping program rejects the 190° values and forms a mean of the remaining values at each grid point. (The 190° values are retained in normal mapping procedures.) At temperatures below 240°K, the difference between this mean and the true target temperature becomes significant, and the error increases as the cutoff temperature is raised and the target temperature is lowered. The error is compensated to some extent by the nonlinear averaging error which is of opposite sign. In fact, the latter may be larger at 240°K. The error caused by the cutoff, however, dominates at low temperatures. Figure 8 shows the combined result of both effects for various cutoff temperatures. The results shown in Figure 8 were computed using actual HRIR noise data. These were combined with radiance values calculated for different target temperatures to simulate the raw digital information. The normal calibration procedure using a fixed cutoff level was then carried out and the resulting temperatures averaged, neglecting values below the cutoff level. The resulting measured mean temperature is plotted on the figure. The departure from true target temperature below 230°K becomes very marked. In fact, the measured mean temperature soon contains little information on actual target temperature and reflects only the cutoff level. For example, with a cutoff temperature of 230°K, the measured mean temperature

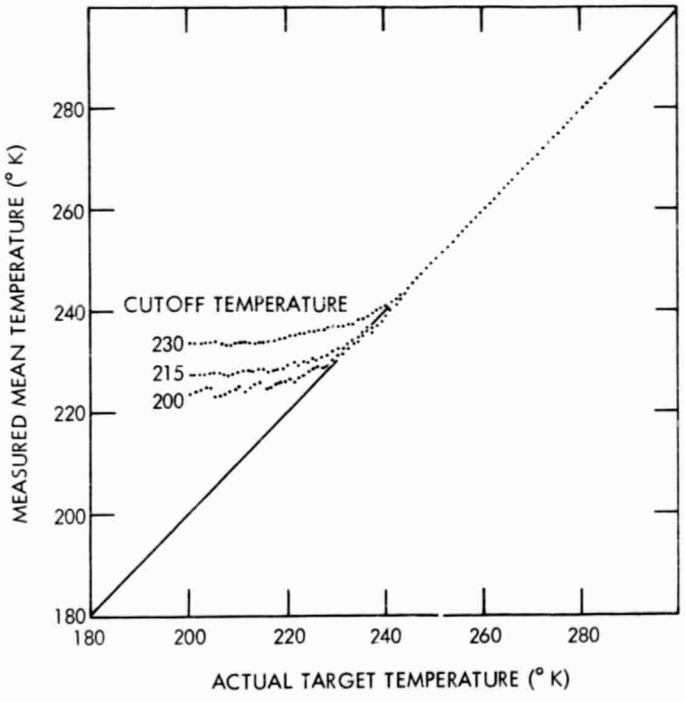

Figure 8—Comparison between actual target temperature and measured mean temperature if the 190°K values are neglected.

is still 233°K even when the instrument views space. In another version, the mapping program retains the 190° values, and, although they are generally lower than the actual brightness temperatures viewed, they often serve to lower the mean grid point temperatures over high, cold clouds to more realistic-appearing values. Also, when mapping at the higher scales (e.g., 1:500,000), the frequency of occurrence and patterns of 190°K values can serve as a diagnostic tool in interpreting the data.

Effect of Temperature-Averaging on Apparent NEΔT

By rejecting data below a cutoff value, measurements subject to the larger negative noise excursions will be removed. The standard deviation of the remaining results therefore will be reduced. Thus the data on the NMRT will appear to have considerably lower NEΔT at low temperatures than is actually the case. This effect is shown in Figure 9, the results having been deduced from synthetic HRIR data in the same way as that described earlier. The full curve, provided for comparison, is the theoretical NEΔT (see Figure 6) without the effect of temperature-averaging. The same effect is shown in actual data. Figure 10 is a scatter diagram on which is

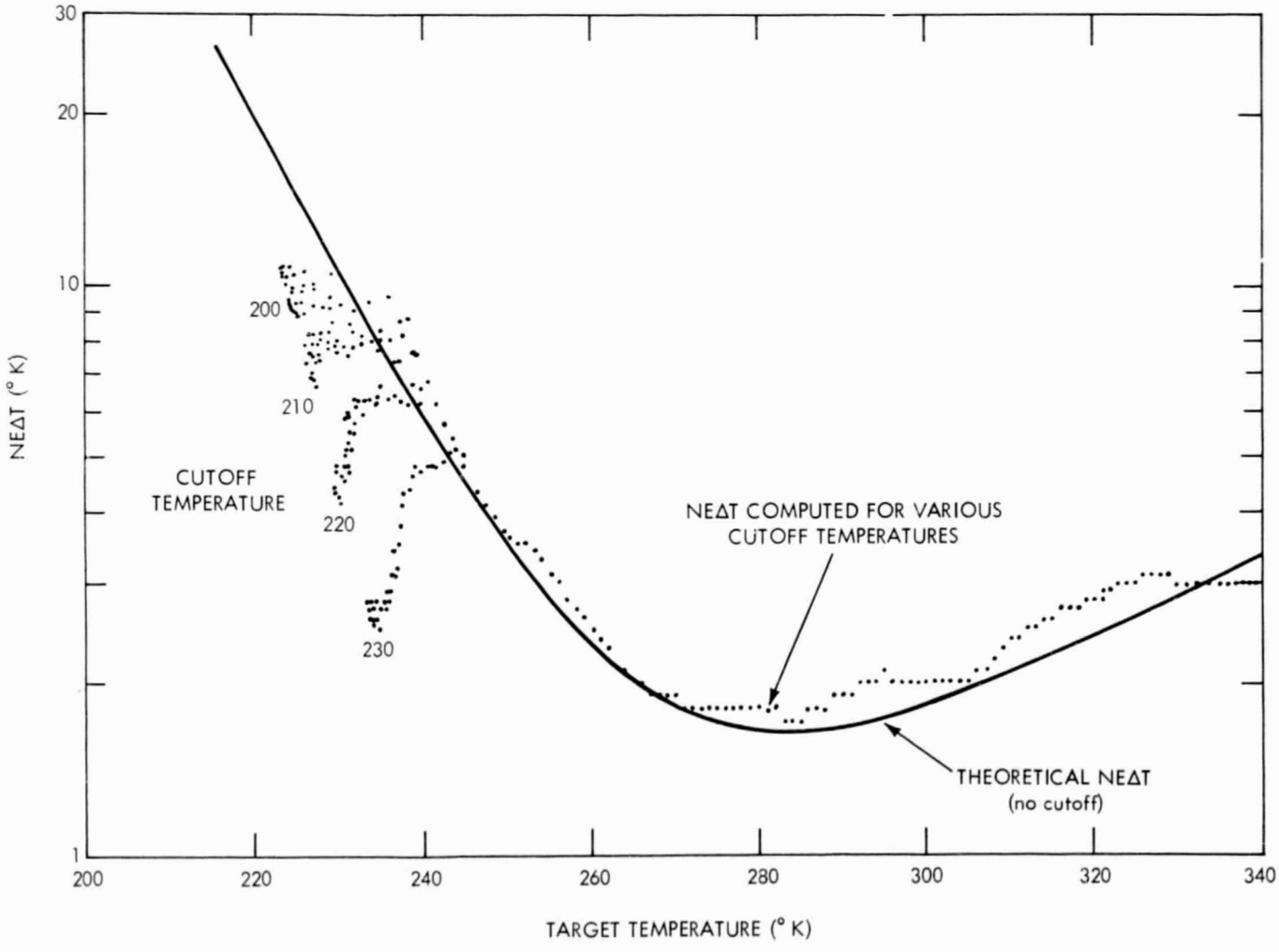

Figure 9—Reduction of apparent NEΔT at low temperatures resulting from rejection of 190°K values.

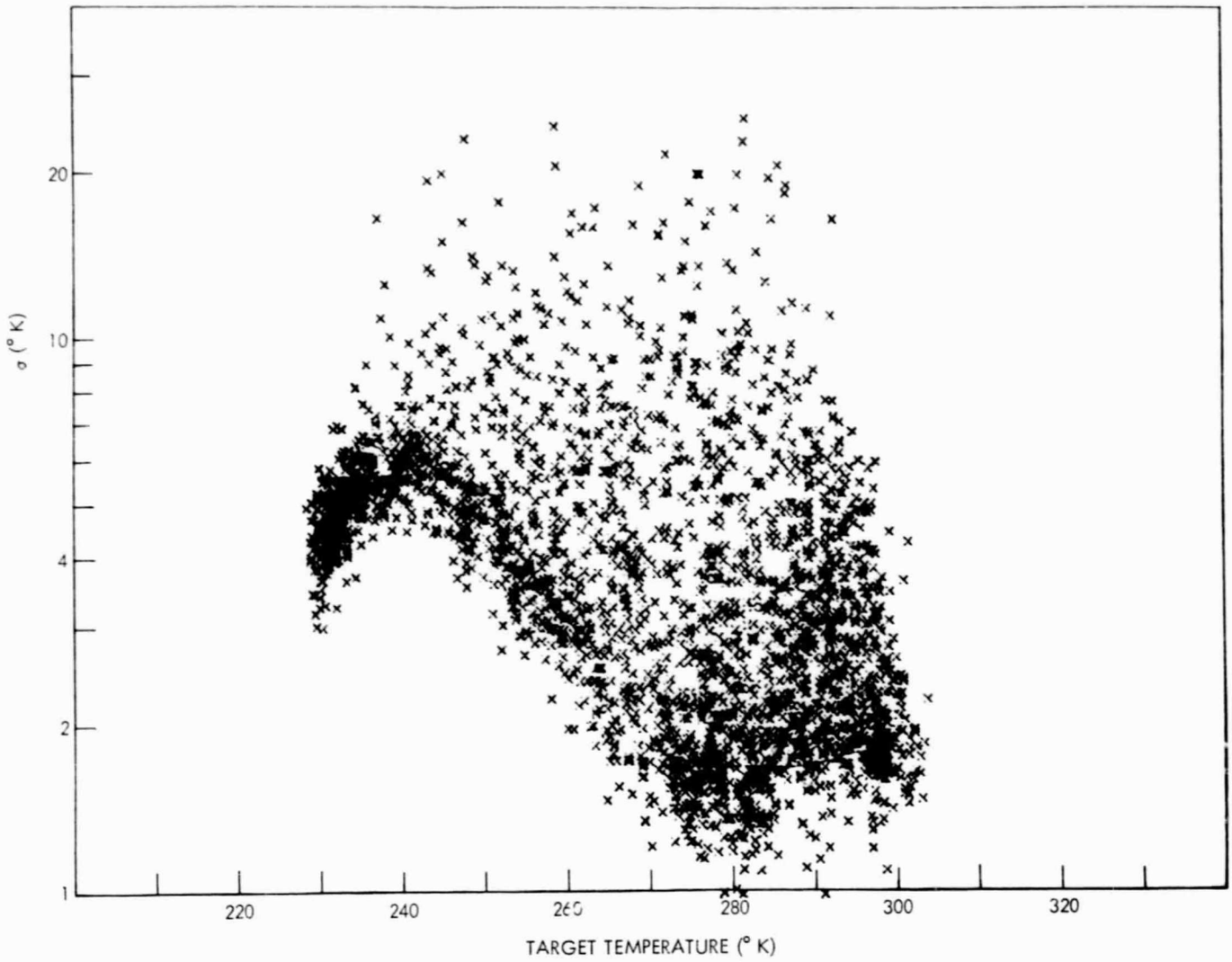

Figure 10—Scatter diagram containing approximately 3000 measurements of the standard deviation of temperature over small regions of the Earth calculated from HRIR data covering one complete day.

plotted approximately 3000 measurements of the standard deviation of temperature over small regions (approx. 60-km diameter) of the earth from NMRT data, plotted against indicated mean target temperature. The standard deviation, in this case, will be a combination of real temperature variation of the target and instrumental noise. The minimum value will clearly represent noise alone and will occur for measurements taken over regions of uniform temperature such as oceans, desert, and ice cap. The lower envelope of the plotted data therefore should indicate the overall effective noise level of the instrument. The effect described earlier can be seen clearly. A second striking feature of Figure 10 is that there are no points plotted below approximately 230°K. This is consistent with the effect illustrated in Figure 8, indicating that a cutoff temperature in the region of 223°K must have been used in the production of the NMRT from which these data were taken.

CONCLUSIONS

Figure 6 expresses the rms variation caused by noise alone in a single HRIR data point as a function of target temperature. The probable error is 0.67 of the value plotted. It can be seen that

below 230°K the value becomes quite large. Noise can be reduced for high temperatures by numerical smoothing, but the practice of averaging temperature rather than radiance values, together with the omission of values below the cutoff temperature, may lead to large systematic errors below 240°K. The value of NEΔT in this region also will appear to be smaller than it really is. These errors are far more serious than those caused by noise because they cannot be reduced by smoothing. Indeed, they are actually introduced by the averaging process used. Numerical filtering techniques are of little use in combating this problem. It can only be solved by introducing new methods of analysis.

Other forms of systematic error have been ignored in this analysis. These will include errors in calibration, errors in measurement of detector and housing temperature, and distortion introduced by the analog recordings and data transmission system.

The purpose of this study has been to investigate the limits of reliability of present HRIR measurements. It is hoped that the results presented will help in a more meaningful interpretation of data at low temperatures. To this end, a number of suggestions are offered.

1. Instrument calibration should be performed at target temperatures 5° apart rather than the intervals of 10° and 20° used in the past.

2. The calibration curve should be made to conform to the shape of the Planck temperature function at the low-temperature end. There are several ways of plotting the data in order to achieve this more readily:

   (a) Temperature on linear scale/digital response on logarithmic scale (as employed in this study)—the graph is practically straight at low temperatures and can be shifted at right angles to the temperature scale to obtain a fit;

   (b) Radiance on a logarithmic scale/digital response on a logarithmic scale—has a slope of unity at low temperatures;

   (c) Radiance on a linear scale/digital response on a linear scale—tends to a straight line through the origin.

In each case, the zero offset has been removed from the data.

3. A more meaningful correction for changes in offset should be incorporated in the data reduction program. With the foregoing calibration scheme, this is achieved simply by subtracting the space level from each measurement.

4. Measurements made during vacuum/thermal tests should be analyzed to assess directly the NEΔT as a function of target temperature. This can be done by examining the earth portion of the scan after digitization of the data.

5. The present scheme of temperature-averaging leads to increasingly large systematic errors below 240°K. To reduce this effect, radiance values should be averaged before conversion to temperature. This will require an alternative format for the NMRT in which data are provided

to the user in the form of radiance rather than temperature. All data points (even those representing negative radiance) should be preserved. Calibration procedures used in the preparation of the revised NMRT would remove the effect of drift by using the space and housing measurements. Basic calibration data would be expressed in terms of radiance units rather than temperature. After performing the necessary averaging, the user would perform the conversion from radiance to temperature. This could probably be done analytically with adequate accuracy since the spectral bandwidth is sufficiently narrow to enable temperature to be represented in terms of a mean Planck function.

The Nimbus II High Resolution Infrared Radiometer has provided a large amount of very useful data. However, because of the vanishingly small amount of energy available at low temperatures in the 3.8-micron window, it is unlikely that high radiometric accuracy can be achieved much below 240°K. Nevertheless, by paying special attention to the sources of error in this region, a realistic estimate of the uncertainty can be obtained, and its magnitude reduced as much as possible.

ACKNOWLEDGMENTS

I am grateful to Messrs. T. T. Cherrix, I. L. Goldberg, and A. W. McCulloch of GSFC and Mr. W. Wallschlaeger of I.T.T. Industrial Laboratories for useful discussions in connection with the instrument. Mr. L. J. Allison provided much of the motivation for the original study.

References

1. Nordberg, W., McCulloch, A. W., Foshee, L. L., and Bandeen, W. R., "Preliminary Results from Nimbus II." *Bull. Amer. Meteor. Soc. 47,* 857, 1966.

2. Staff Members, Laboratory for Atmospheric and Biological Sciences, 1966: Nimbus I High Resolution Radiation Data Catalog and Users Manual: Volume 2, Nimbus Meteorological Radiation Tapes—HRIR. National Space Science Data Center, Goddard Space Flight Center, NASA, Greenbelt, Md.

3. Warnecke, G., Allison, L. J., Kreins, E. R., and McMillin, L. M., "A Tropical Cyclone Development as Revealed by Nimbus II High Resolution Infrared and ESSA-3 Television Data," Proceedings of the V Conferencia Tecnia De Huracanes Y Meteorologia Tropical, Caracas, Venezuela, Nov. 1967 (also available as GSFC document X-622-68-39).

4. Warnecke, G., Allison, L. J., Foshee, L. L., "Observations of Sea Surface Temperatures and Ocean Currents from Nimbus II," Space Research VIII, North-Holland Publishing Co., Amsterdam, pp. 1016-1023 (also available as GSFC document X-622-67-435).

5. McMillin, Larry M., 1969: "A Procedure to Eliminate Periodic Noise Found in Nimbus II High Resolution Infrared Radiometer Measurements," Allied Research Associates Technical Report No. 9, Contract NAS5-10343 with NASA Goddard Space Flight Center, Greenbelt, Md.